Circulation Research

ORIGINAL RESEARCH

CARMN Loss Regulates Smooth Muscle Cells and Accelerates Atherosclerosis in Mice

Francesca Vacante, Julie Rodor, Mukesh K. Lalwani, Amira D. Mahmoud, Matthew Bennett, Azzurra L. De Pace, Eileen Miller, Kim Van Kuijk, Jenny de Bruijn, Marion Gijbels, Thomas C. Williams, Michael B. Clark, Jessica P. Scanlon, Amanda C. Doran, Rusty Montgomery, David E. Newby, Mauro Giacca, Dónal O'Carroll, Patrick W.F. Hadoke, Laura Denby,* Judith C. Sluimer,* Andrew H. Baker

RATIONALE: In the microenvironment of atherosclerotic lesions, vascular smooth muscle cells (vSMCs) switch to a dedifferentiated state but the underlying molecular mechanisms driving this switch are not fully understood. Long noncoding RNAs (lncRNAs) are dysregulated during vascular pathology, but relatively little is known about their involvement in controlling vSMCs function. Cardiac mesoderm enhancer-associated noncoding RNA (CARMN) is a lncRNA located immediately upstream of the *microRNAs-143* and-*145 (miR-143* and *miR-145)*, both involved in vSMCs function.

OBJECTIVE: We investigated the role of the lncRNA CARMN, independent from miR-143 and miR-145, as a potential regulator of vSMC phenotypes in vitro and the consequences of its loss during the development of atherosclerosis in vivo. We hypothesized that loss of CARMN is a primary event controlling the functional switch towards proatherogenic vSMC phenotype and accelerates the development of the plaques in vivo.

METHOD AND RESULTS: Expression of CARMN lncRNA was silenced using locked nucleic acids antisense oligonucleotides (GapmeRs) in human coronary arterial smooth muscle cells, revealing that GapmeR-mediated loss of CARMN negatively affects miR-143 and miR-145 microRNA expression. RNA sequencing of CARMN-depleted human coronary arterial smooth muscle cells revealed large transcriptomic changes, associated with vSMC proliferation, migration, inflammation, lipid metabolism, and dedifferentiation. The use of miR-143 and miR-145 mimics revealed that CARMN regulates human coronary arterial smooth muscle cell proliferation in a microRNA-independent manner. In humans and mice, CARMN and associated microRNAs were downregulated in advanced versus early atherosclerotic lesions. Using a CRISPR (clustered regularly interspaced short palindromic repeats)-Cas9 (CRISPR-associated protein 9) knockout approach, we explored the implications of *CARMN* depletion during atherosclerosis in vivo. Consistent with in vitro results, the knockout of *CARMN* impaired the expression of miR-143 and miR-145 under homeostatic conditions. Importantly, when atherosclerosis was induced in these mice, CARMN knockout increased the volume, size, proinflammatory Lgals3 (galectin 3)-expressing cells content, and altered plaque composition, yielding an advanced phenotype.

CONCLUSIONS: We identified the early loss of CARMN lncRNA as critical event which primes vSMCs towards a proatherogenic phenotype in vitro and accelerates the development of atherosclerosis in vivo.

GRAPHIC ABSTRACT: A graphic abstract is available for this article.

Key Words: atherosclerosis ■ cell proliferation ■ cholesterol ■ inflammation ■ phenotype

Editorial, see p 1276 | In This Issue, see p 1237 | Meet the First Author, see p 1238

Atherosclerosis is a chronic and inflammatory condition of the arterial branches and a leading cause of cardiovascular disease and cerebrovascular disease.[1] Vascular smooth muscle cells (vSMCs) have a critical and complex role in atherogenesis. In homeostatic conditions, adult vSMCs are largely quiescent and

Correspondence to: Andrew H. Baker, PhD, University of Edinburgh, Queen's Medical Research Institute, 47 Little France Crescent, Edinburgh, United Kingdom. Email andy.baker@ed.ac.uk

*L. Denby and J.C. Sluimer contributed equally.

The Data Supplement is available with this article at https://www.ahajournals.org/doi/suppl/10.1161/CIRCRESAHA.120.318688.

For Sources of Funding and Disclosures, see page 1274.

Novelty and Significance

What Is Known?

- Dedifferentiation of vascular smooth muscle cells (vSMCs) occurs in atherosclerotic lesions.
- Noncoding RNAs, such as long noncoding RNAs (lncRNAs) and microRNAs (miRNAs), can regulate key aspects of vascular pathology.
- Cardiac mesoderm enhancer-associated noncoding RNA (CARMN) is a lncRNA located immediately upstream of *miRNAs, microRNAs-143* and-*145 (miR-143* and *miR-145)*, which are involved in vSMC function.

What New Information Does This Article Contribute?

- The CARMN/miR-143/miR-145 axis can prime vSMCs towards proproliferative, promigratory, and dedifferentiated phenotypes, in vitro.
- CARMN lncRNA potentially acts independently of the miRNAs to regulate vSMC proliferation, whereas migration and dedifferentiation phenotypes are likely modulated by miR-143/145 independently.
- *CARMN* knockout mice develop accelerated atherosclerosis and advanced plaques.

In this study, the conserved and genetically complex long noncoding RNA CARMN, and its colocated miRNAs, miR-143 and miR-145, were comprehensively characterized in human and mouse atherosclerosis. CARMN transcript downregulation was associated with advanced plaque phenotype and *CARMN* knockout in mice had increased atherosclerosis. Downregulation of the CARMN/miR-143/miR-145 axis primed vSMCs towards proproliferative, promigratory, and dedifferentiated phenotypes, in vitro. Mechanistically, we provided evidence that the CARMN lncRNA acted independently of the miRNAs to regulate vSMC proliferation, whereas migration and dedifferentiation phenotypes were associated with the modulation of miRNAs expression. Although both miRNAs are well known in vSMC biology, our study begins to dissect the complex genetic interplay between lncRNA host genes and their associated miRNAs in health and disease. Furthermore, we provide evidence for the fundamental, yet complex role of lncRNAs in vSMC function.

Nonstandard Abbreviations and Acronyms

Acta2	actin alpha 2
CARMN	cardiac mesoderm enhancer-associated noncoding RNA
CARMN$^{-/-}$	CARMN knockout
CARMN$^{+/+}$	CARMN wild-type
CCL	chemokine C-C motif ligand
CMBCD	cholesterol-methyl-β-cyclodextrin
CXCL1	C-X-C motif chemokine 1
hCASMCs	human coronary artery smooth muscle cells
IL	interleukin
Lgals3	galectin 3
lncRNA	long noncoding RNA
MiRNAs	microRNAs
MMP1	matrix metalloproteinase 1
Myocd	myocardin
Ox-LDL	oxidized low-density lipoprotein
PCSK9	proprotein convertase subtilisin/kexin type 9
PDGF	platelet-derived growth factor
qRT-PCR	quantitative real-time polymerase chain reaction
UBC	ubiquitin C
vSMCs	vascular smooth muscle cells
αSMA	α-smooth muscle actin

characterized by a specific gene expression pattern and functional properties which define their signature.[2] However, in response to pathological environmental stress signals that occur during atherogenesis, vSMCs lose their contractile signature and switch into a proatherogenic phenotype as they start to proliferate, migrate, and lose their typical markers (such as smooth muscle actin alpha 2).[3–5] In particular, during the formation of stable plaques, vSMC proliferation and migration toward the intimal layer are associated with the formation of a stabilizing fibrotic cap.[6] Whereas, during the latter stages of disease, the recruitment and activation of inflammatory cells, the decrease in collagen content, and increase in metalloprotease secretion contribute to the breakdown and dynamic remodeling of the fibrotic cap and the progression towards rupture-prone plaques.[7] Therefore, it is critical to unravel and fully understand these complex regulatory networks to be able to target specific molecular mechanisms during the progression of atherosclerosis.

Recently, several studies have demonstrated that noncoding RNAs, namely long noncoding RNAs (lncRNAs) and microRNAs (miRNAs), are crucial regulators of many pathophysiological processes during atherosclerosis.[8–10] MiRNAs namely *microRNAs-143* and-*145 (miR-143* and *miR-145)*, have been found to be important regulators of vSMC differentiation and disease-associated phenotypic switching in response to proatherogenic stimuli, such as cholesterol loading (water-soluble cholesterol)[11] or PDGF (platelet-derived growth factor)-BB treatment.[12–16] Their

functions have also been highlighted in several mouse models, where the ablation of both, *miR-143* and *miR-145*, induced spontaneous neointimal lesions in the femoral artery,[14,17] dysregulated signaling pathways,[14] and regulated vSMC migration.[17] However, despite numerous studies uncovering the importance of miR-143 and miR-145 in diverse disease conditions,[14–16,18–22] their function and regulation remain conflicting in the context of atherosclerosis.[16,19]

A long noncoding RNA (lncRNA), named cardiac mesoderm enhancer-associated noncoding RNA (CARMN), is juxta-positioned upstream from *miR-143 and miR-145*.[23] This lncRNA was originally identified in human cardiomyocytes.[24,25] Previous studies have demonstrated that a crosstalk may exist between the processing of lncRNA host genes, such as CARMN, and encoded miRNAs[26] and that the biogenesis of these noncoding molecules might be mutually exclusive[27] and produced RNAs with independent functions.[28] Although the functions of miR-143 and miR-145 have been explored, whether CARMN has an independent function is not completely elucidated in the context of atherosclerosis. Here, we demonstrated that CARMN has a function independent from miR-143 and miR-145 in regulating vSMC proliferation, whereas vSMC migration or dedifferentiation processes are regulated through the modulation of miRNA expression in human coronary arterial smooth muscle cells (hCASMCs). Moreover, we uncovered a pivotal role of the *CARMN/miRNAs* locus during the pathophysiology of atherosclerotic disease in vivo and demonstrated that in *CARMN* knockout mice, the development of atheroma was accelerated when compared with wild-type mice, thereby inducing advanced and more vulnerable plaques.

METHODS

Data Availability

Expanded information about materials and methods are available in the Data Supplement. All supporting data and materials are available within the Data Supplement and available from the corresponding author upon reasonable request. All RNA sequencing data are deposited in the Gene Expression Omnibus database (Ref. GSE158972 and Ref. GSE165445).

RESULTS

Expression and Subcellular Localization of CARMN lncRNA and Associated miRNAs in Primary Human CASMCs Under Basal and Stimulated Conditions

We first sought to understand the expression and regulation of *CARMN* in hCASMCs together with miRNAs miR-143 and miR-145miR-143 and miR-145 Ensembl database 98 show several transcript variants belonging to the complex *CARMN* locus (Figure 1A). Initially, we assessed the expression levels of individual isoforms in hCASMCs, using isoform-specific primers when possible (only isoform 4 was amplified in combination with isoform 9; Figure 1A). Expression data indicated that all the isoforms were detectable in hCASMCs (Figure 1B). Following this, we used common primers capturing all isoforms, except 205 and 211, to assess the expression levels of *CARMN* (Figure 1A). Based on previous studies, the function of lncRNAs is related to their subcellular localization[29,30]; therefore, we next determined the localization of CARMN in hCASMCs. Subcellular fractionation as well as RNA–fluorescent in situ hybridization indicated that CARMN predominantly localized in the nuclear compartment of hCASMCs (Figure IA and IB in the Data Supplement). Of note, during the course of these experiments, there was a new release of the Ensembl annotation that included 7 new potential isoforms (Figure IIA in the Data Supplement), yet all remained detectable by our common primer set. However, considering that lncRNA annotation is not definitively accurate and that lncRNA are expressed in a cell-specific way, we applied a transcript discovery pipeline to publicly available RNA-Seq data of hCASMCs obtained by ENCODE (Encyclopedia of DNA Elements) (https://www.encodeproject.org/), which did not reveal the existence of un-annotated additional isoforms (Figure IIA in the Data Supplement). This analysis also showed that the 3′ end of the most abundant *CARMN* transcripts is upstream of the *miR-143/miR145* loci (Figure IIA in the Data Supplement). Moreover, we carried out 5′ Rapid Amplification of cDNA ends and long-reads sequencing (Oxford Nanopore technology). Both techniques not only revealed the presence of a main transcriptional start site, already described in the annotation, but also detected minor additional transcriptional start sites (Figure IIB and IIC in the Data Supplement). Moreover, the long-read sequencing revealed 4 major exonic structures, all covered by the current annotation and not including *miR-143/145* (Figure IID in the Data Supplement). In addition, we found reads mapping to the *miR-143/miR-145* stem-loop which suggested the existence of fragments from the processed primary miRNA transcript (pri-miRNA) with different 5′ end, one of them shared by *CARMN* transcripts (Figure IIE in the Data Supplement). Altogether, these analyses confirmed the complexity of *CARMN* locus.

PDGF-BB is one of the main pathogenic cytokines released at the site of injury with a potent mitogen action to vSMCs.[31] To gain insight into the regulation of *CARMN* in proliferating VSMCs, we treated serum-starved hCASMCs with PDGF-BB for 48 hours (Figure 1C) and assessed the levels of CARMN was significantly downregulated following PDGF-BB stimulation (Figure 1D). Levels of expression of miR-143 and miR-145 were also significantly decreased (Figure 1D). It is well established that vSMC migration from the media to the intima is critically involved in the pathophysiology of vascular disease,

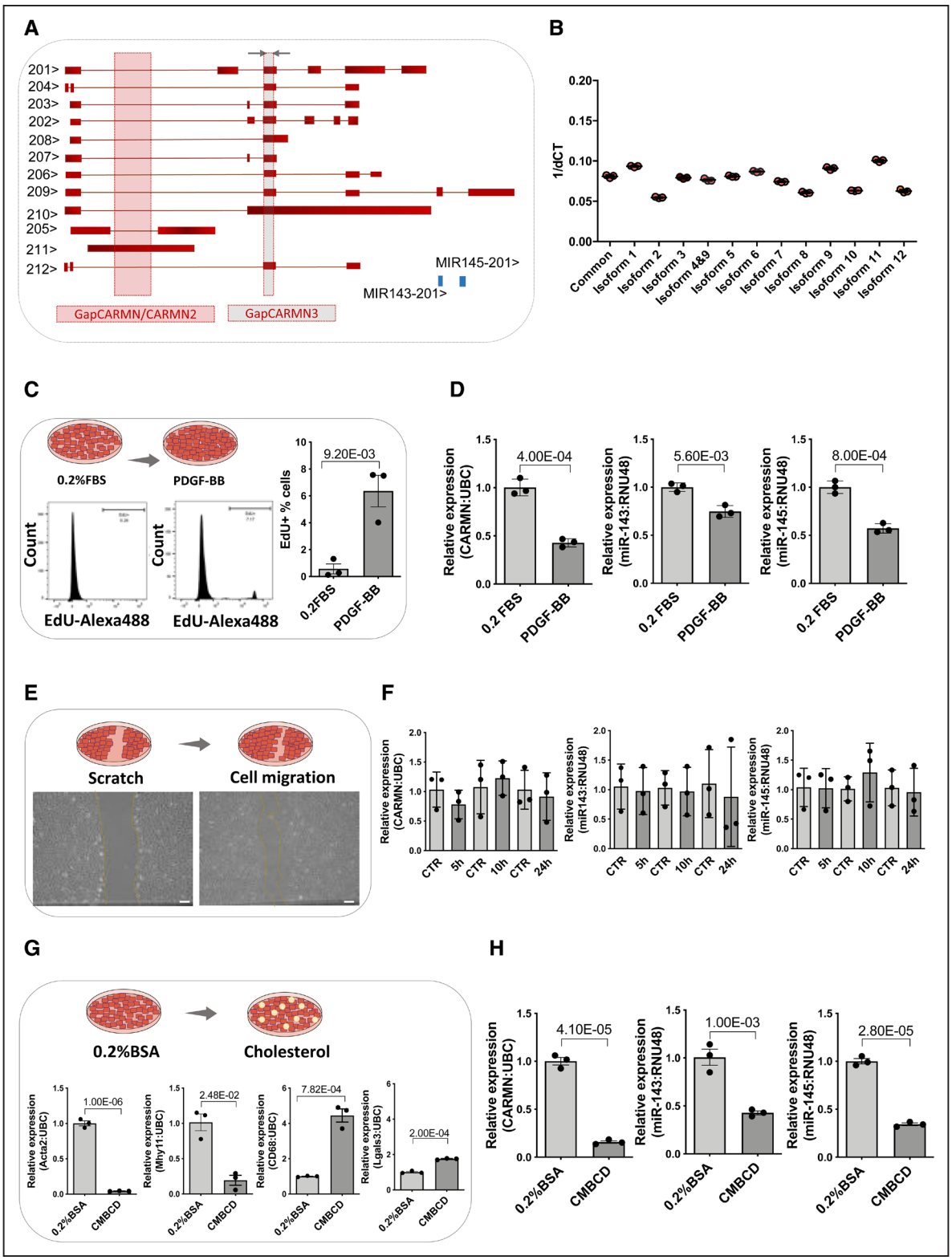

Figure 1. Cardiac mesoderm enhancer-associated noncoding RNA (CARMN) expression in basal and stimulated human primary coronary arterial smooth muscle cells (CASMCs).

A, Schematic representation of human *CARMN* splice variants and premicroRNAs of microRNA-143 and -145 (miR-143 and miR-145) based on ENSEMBL version 98 including the position of the forward (Fw) and reverse (Rev) primers used to amplify all transcripts, gray arrows (except 4, 10 and 11) and the target region for the GapmeRs (locked nucleic acids antisense oligonucleotides), targeting CARMN, GapCARMN, GapCARMN2 and GapCARMN3. The black arrows next to each transcript name, indicate the direction of transcription. **B**, Expression levels of CARMN transcripts in human CASMCs (hCASMCs; n=3) via quantitative real-time polymerase chain reaction (qRT-PCR) using isoform-specific primers (isoform 1, 2, 3, 4+9, 5, 6, 7, 8, 9, 10, 11, and 12) and common primers (amplifying all isoforms except 4, 10, and 11). **C**, Diagram of hCASMCs in basal condition (0.2% FBS) and treated for 48 h with PDGF (*Continued*)

although it is a difficult process to be quantified in human lesions.[4] We, therefore, assessed whether CARMN was dynamically regulated under migratory stimuli. A scratch was made in a monolayer of serum-starved hCASMCs, and the levels of CARMN and miR-143/145 were assessed at 5, 10, and 24 hours after scratching (Figure 1E). However, no statistical difference was observed in the lncRNA or microRNAs expression in scratched versus control cells (Figure 1F). Additionally, we characterized the expression of the lncRNA CARMN in primary culture of hCASMCs following the treatment with water-soluble cholesterol-methyl-β-cyclodextrin (CMBCD), for 72 hours (Figure 1G). CMBCD loading substantially decreased the expression levels of CARMN versus control cells, and similarly, the expression of miR-143 and miR-145 (Figure 1H), as previously described.[11] Moreover, we observed similar pattern of decrease in CARMN expression using another model of hCASMC dedifferentiation towards foamy cell–like phenotype[32] by loading cells with ox-LDL (oxidized low-density lipoprotein; Figure IIIA through IIIC in the Data Supplement). Thus, the expression levels of CARMN lncRNA and associated miRNAs are reduced by the exposure to proliferative stimuli and CMBCD loading of hCASMCs, which is a critical process during the pathophysiology of atherosclerosis.

Knockdown of the Human CARMN-Axis Drives the Phenotypic Transition of hCASMCs Towards a Proatherogenic Phenotype

To assess the functional importance of CARMN, we utilized an GapmeRs (locked nucleic acids antisense oligonucleotides) approach. We designed 2 different GapmeRs targeting the introns of CARMN isoforms (named GapCARMN and GapCARMN2; Figure 1A). Following transfection of hCASMCs with GapCARMN and GapCARMN2, we observed a significant knockdown of CARMN versus a GapmeR control (GapCTR) using the common primers (Figure 2A, Figure IIID in the Data Supplement). Importantly, we confirmed the downregulation of CARMN at the isoform level using isoform-specific primers (Figure IIIE in the Data Supplement). Notably, the levels of miR-143 and miR-145 were also significantly downregulated following GapCARMN and GapCARMN2 transfection in CASMCs (Figure 2A and Figure IIID in the Data Supplement). Furthermore, to support the results obtained with intronic-targeting GapmeR (GapCARMN/GapCARMN2), we used a previously described GapmeR targeting the exonic region of CARMN transcripts (named GapCARMN3 in this manuscript)[25] and confirmed similar changes (Figure IVA in the Data Supplement).

To understand the role of CARMN in hCASMCs in physiological and pathological conditions, we analyzed the transcriptomic changes associated with the CARMN-axis depletion using GapCARMN in untreated hCASMCs (basal), as well as following stimulation upon proliferation, migration, or CMBCD loading (Figure 2B). The expression of CARMN was firstly assessed in RNA sequencing samples to validate appropriate knockdown (Figure IVB in the Data Supplement). Following RNA sequencing analysis, principal component analysis confirmed clustering of the sample replicates and showed a clear separation of the GapCARMN-treated samples from the GapCTR-treated hCASMCs in all analyzed conditions (Figure IVC in the Data Supplement). The principal component analysis also confirmed an effect of the different treatments at the transcriptomic level. In particular, we noted the clear separation of the CMBCD-treated cells from their relevant control cells (Basal_C), showing the strong effect of this stimulus on the hCASMC transcriptome. We also noticed the proliferation-stimulated samples showed an intermediate phenotype which can be explained by different responses due to the diverse cell culture densities of the hCASMCs, as well as the point of harvesting following GapmeR transfection. We analyzed the significant changes in gene expression in GapCARMN versus GapCTR-treated cells for each condition (Figure IVD in the Data Supplement) and found that CARMN depletion affected a large number of genes, on average 910 genes per condition with 411 upregulated and 499 downregulated genes. In total, we found 2315 genes whose expression was significantly changed by CARMN depletion and analyzed their expression profiles (Figure 2C). The heatmap revealed a largely consistent effect of CARMN-axis depletion, independent of hCASMC treatment. Gene ontology analysis of the CARMN-axis–dependent genes in basal conditions already revealed the enrichment of several processes related to vSMC phenotypic transition towards dedifferentiated phenotype (Figure 2D). More specifically, we noted enrichment of terms linked to a positive effect on

Figure 1 Continued. (platelet-derived growth factor)-BB. Histogram plots obtained by fluorescence-activated cell sorting (FACS) showing the percentage of hCASMCs (n=3) up-tacking 5-ethynyl-2'-deoxyuridine (EdU) following PDGF-BB treatment and in basal (0.2% FBS) conditions. Student *t* test was used to assess statistical significance indicated with *P* values. **D**, qRT-PCR to show expression of CARMN, miR-143, and miR-145 in hCASMCs (n=3) treated with PDGF-BB. Student *t* test was used to assess statistical significance indicated with *P* values. **E**, Diagram of the wound healing assay performed in hCASMCs (n=3), **F**, representative micrographs of hCASMCs scratch assay and migrating cells (Scale bar 100 μm) and qRT-PCR showing the expression of CARMN and miR-143/145. in CTR (control) and scratched. **G**, Diagram of hCASMCs (n=3) in basal condition (0.2% BSA) and treated with cholesterol-methyl-b-cyclodextrin treated for 72 h and expression levels of dedifferentiation markers (ACTA2 [actin alpha 2], MYH11 [myosin heavy chain 11], CD68 [cluster of differentiation 68], and LGALS3 [galectin 3]), CARMN and miR-143/145 by qRT-PCR. Student *t* test was used to assess statistical significance indicated with *P* values. **H**, QRT-PCR data showing the expression of CARMN and miR-143/145 in basal (0.2% FBS) and following cholesterol-methyl-β-cyclodextrin (CMBCD)-loading treatment. Student *t* test was used to assess statistical significance indicated with *P* values. UBC indicates ubiquitin C.

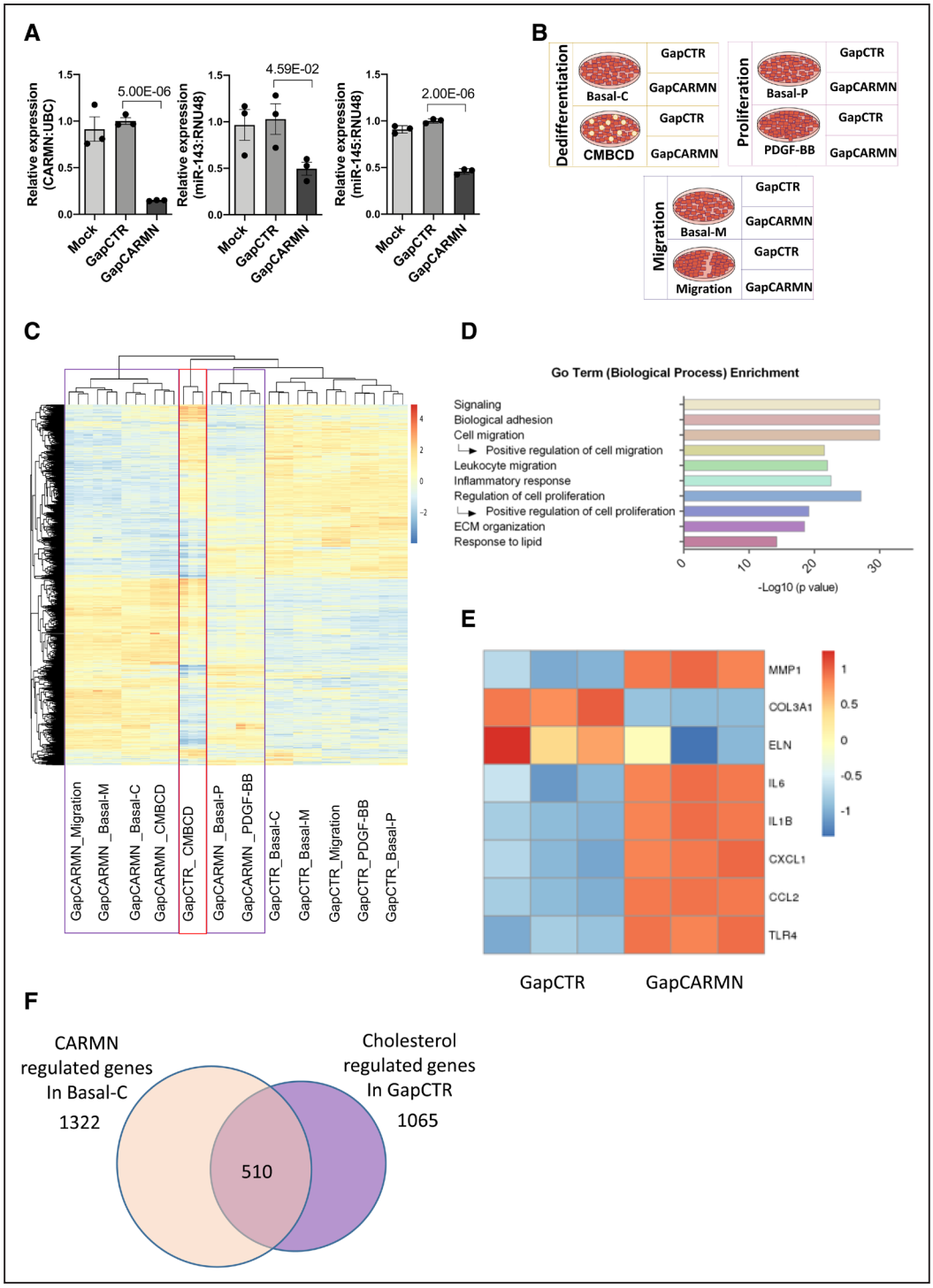

Figure 2. Cardiac mesoderm enhancer-associated noncoding RNA (CARMN)–regulated genes relevant to vascular smooth muscle cell proliferation, migration, and water-soluble cholesterol–dependent dedifferentiation.
A, Quantitative real-time polymerase chain reaction results showing the expression of CARMN, microRNAs-143 and -145 (miR-143 and miR-145) human coronary arterial smooth muscle cells (hCASMCs; n=3) following transfection with locked nucleic acids antisense oligonucleotides (GapmeRs) targeting CARMN (GapCARMN) and GapmeR control (GapCTR). Mock indicates untransfected cells. One-way ANOVA with Bonferroni multiple comparison test was used to assess statistical significance indicated with *P* values. **B**, Schematic representation of the RNA sequencing study design. **C**, Heatmap (as *Z* score of log2[FPKM, Fragments Per Kilobase of transcript per Million mapped reads +1]) of differentially regulated genes by CARMN depletion in all conditions. The purple box highlights the clustering of all CARMN_KD samples, whereas the red box shows the cholesterol-methyl-β-cyclodextrin (CMBCD)–treated replicates in control knockdown (Cont_KD). **D**, Graph of selected Go Term (Biological Process). The analysis was performed on the 2315 genes regulated by CARMN depletion in any conditions. **E**, Heatmap (as *Z* score of log2[FPKM+1]) of selected differentially regulated genes by GapCARMN and GapCTR in the basal condition with the shortest time of GapmeR transfection (migration). **F**, Venn diagram showing the overlap between genes regulated by CARMN depletion (in Basal-C condition) and genes regulated by CMBCD treatment (in GapCTR condition) in the same direction. ECM indicates extracellular matrix; PDGF, platelet-derived growth factor; and UBC, ubiquitin C.

cell migration and proliferation that are key processes during atherogenesis. Moreover, we investigated whether the depletion of CARMN-axis affects the transcription factor regulating vSMC homeostasis, MYOCD (myocardin).[33] However, MYOCD was undetectable in both, our RNA sequencing and by quantitative real-time polymerase chain reaction (qRT-PCR) analysis (Figure IVE and IVF in the Data Supplement). Interestingly, CARMN-dependent genes were also involved in lipid metabolism and cholesterol homeostasis. CARMN depletion also upregulated the expression of proinflammatory cytokine genes such as interleukins; IL1-beta, IL6) associated with atherosclerosis progression and CXCL1 (C-X-C motif chemokine 1) and as well as CCL2 (chemokine C-C motif ligand 2) chemokines, responsible for leucocyte migration and recruitment to the developing lesions (Figure 2E).[34,35] Furthermore, we noted a significant upregulation of MMP1 (matrix metalloproteinase 1) and a significant downregulation of collagen and elastase genes COL3A1 (collagen type 3 alpha chain 1) and ELN (elastase), with expression decreasing in the context of extracellular matrix remodeling and plaque vulnerability (Figure 2E).[36,37] Genes regulated by CARMN and involved in positive regulation of proliferation, migration, regulation of inflammatory response, and response to lipid are reported in Data set II in the Data Supplement. Related to the enrichment of lipid terms in the gene ontology analysis, the heatmap of CARMN-regulated genes revealed the clustering of CMBCD-treated samples transfected with GapCTR among all GapCARMN samples, further suggesting that CARMN-dependent genes were also affected by CMBCD treatment (Figure 2C). Therefore, we directly compared the genes regulated by CARMN in basal condition with genes changed upon CMBCD treatment. Importantly, we found that about 50% of CMBCD-regulated genes were altered in the same direction upon CARMN depletion (Figure 2F), suggesting that CARMN depletion alone promotes a water-soluble cholesterol loaded–like phenotype in the absence of CMBCD treatment. These results show the impact of CARMN depletion on hCASMCs transcriptome and in particular on cholesterol-regulated genes. Collectively, these results suggest CARMN knockdown might be an important event which primes vSMCs to the phenotypic transition occurring in plaques formation and progression.

Knockdown of CARMN-Axis lLncRNA Activates Proliferation, Migration and Induces Partial Dedifferentiation of hCASMCs In Vitro

Considering the results obtained from the transcriptomic analysis of CARMN silenced hCASMCs, we further deciphered the functional consequence of CARMN-axis silencing on hCASMC phenotypes. Interestingly, the depletion of CARMN significantly increased the proliferation of hCASMCs in quiescent conditions (0.2%FBS) or under PDGF-BB stimulation (Figure 3A and 3B). Next, we assessed the effect of CARMN depletion on hCASMC migration. Although the response to the migratory stimulus did not show significant difference in the expression levels of endogenous CARMN and miR-143/145, the downregulation of CARMN increased the migration rate of hCASMCs versus cells transfected with GapCTR (Figure 3C and 3D). To further validate the involvement of CARMN in hCASMC CMBCD-induced dedifferentiation process, we analyzed mRNA expression changes of the smooth muscle identity markers, ACTA2 (actin alpha 2) and MYH11 (myosin heavy chain 11), and activated macrophage-like genes, CD68 (cluster of differentiation 68) and Lgals3 (galectin-3). We confirmed that CARMN depletion leads to significant decrease of ACTA2 and MYH11 levels, with concomitant significant increase of CD68 expression in basal conditions (Figure 3E, 3F, and 3G). However, we did not observe significant change in LGALS3 expression in CARMN-depleted hCASMCs when compared to control group (Figure 3H). Moreover, we assessed the expression levels of KLF4 (Kruppell-like factor 4) in CARMN-depleted hCASMCs, previously associated with vSMC dedifferentiation phenotype.[38] We did not observe significant change in the expression of this transcription factor in CARMN-depleted proliferative or dedifferentiating hCASMCs (Figure VA and VB in the Data Supplement), indicating likely KLF4-independent effects. Instead, we observed a significant increase in KLF4 in scratched hCASMCs with CARMN depletion (Figure VC in the Data Supplement). To robustly characterize hCASMCs phenotypic state following CARMN depletion, we also took into consideration other typical vSMCs marker genes such as *CNN1* (calponin1) and *TAGLN* (taglin).[39,40] However, their expression levels were not significantly changed following CARMN-axis knockdown (Figure VD and VE in the Data Supplement), therefore, indicating that CARMN downregulation partially affects the vSMCs signature under unstimulated conditions. In addition, we investigated the expression of lipid metabolism–associated genes, such as *ABCA1* (ATP-binding cassette transporter 1) and *ABCG1 (ATP-binding cassette subfamily G member 1),*[11] which were found significantly upregulated following CARMN knockdown versus control (Figure VF and VG in the Data Supplement). We did not observe the same pattern in the case of SREBPF2 (Sterol Regulatory Element Binding Transcription Factor 2), *SCD* (Stearoyl-CoA Desaturase), and *HMGS1* (3-hydroxy-3-methylglutary -CoA synthase 1) expression (Figure VH, VI, and VJ in the Data Supplement), indicating that the modulation of CARMN partially primes the dedifferentiation towards a proinflammatory phenotype foam cell–like phenotype. These phenotypic changes observed in hCASMCs, were confirmed with a second

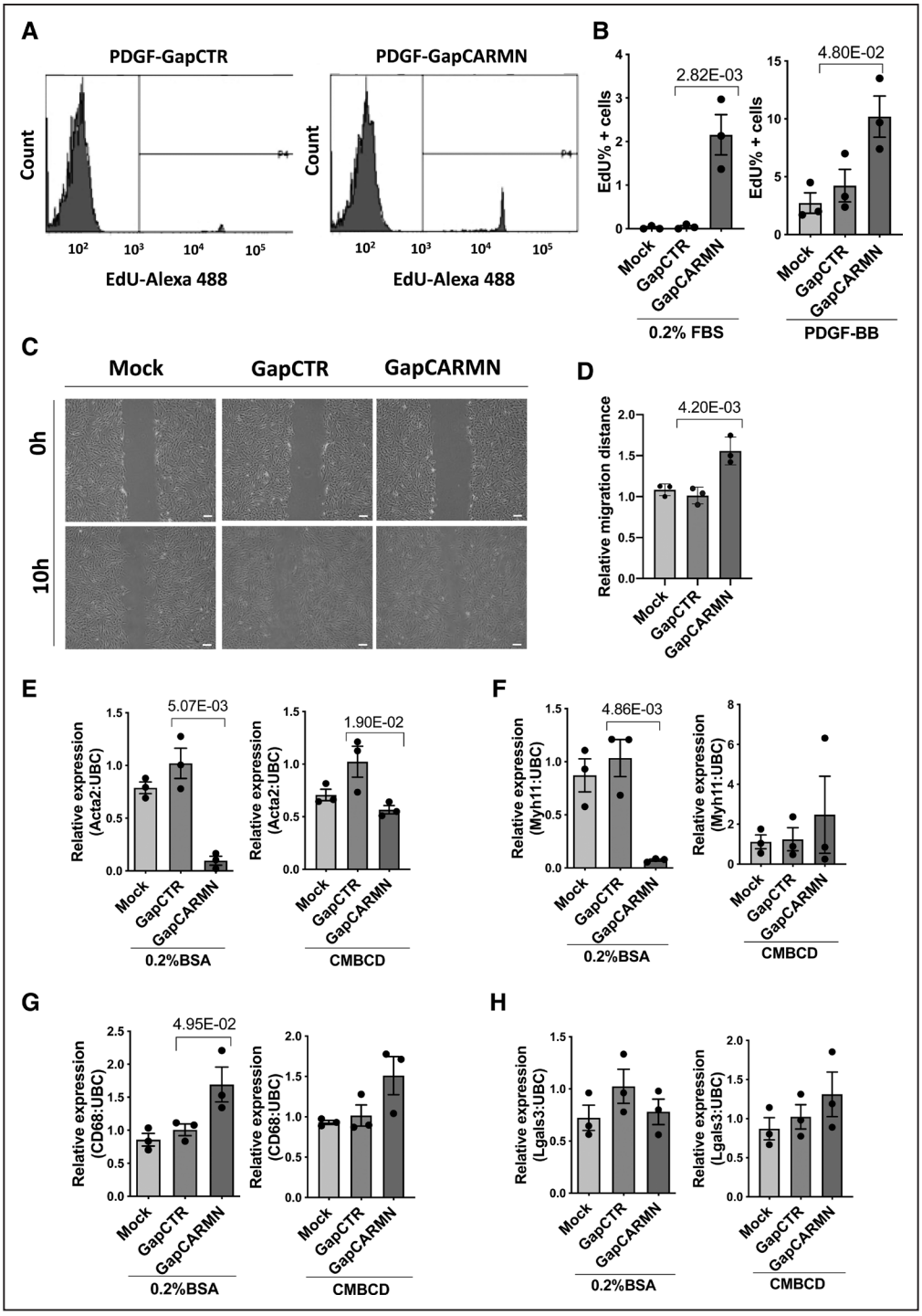

Figure 3. The knockdown of cardiac mesoderm enhancer-associated noncoding RNA (CARMN) regulated human coronary arterial smooth muscle cell (hCASMC) proliferation, migration, and dedifferentiation.

A, Representative fluorescence-activated cell sorting (FACS) plots showing the 5-ethynyl-2'-deoxyuridine (EdU) uptake in hCASMCs transfected with locked nucleic acids antisense oligonucleotides (GapmeRs) targeting CARMN (GapCARMN) or GapmeR control (GapCTR). The gate (P4) indicates the EdU-positive cells; the samples are named GapmeR negative control (GapCTR) and GapmeR targeting CARMN (GapCARMN). **B**, Percentage of EdU-positive hCASMCs (n=3) following transfection with GapCARMN, GapCTR, and untransfected cells (Mock) upon PDGF (platelet-derived growth factor)-BB stimuli and in 0.2% FBS. One-way ANOVA with Bonferroni multiple comparison test was used to assess statistical significance indicated with *P* values. **C**, Representative pictures of hCASMCs at 0 and 10 h from the scratch following transfection with GapCARMN, GapCTR, and Mock in 0.2% FBS medium. Pictures were acquired at ×10 magnification. Scale bar 100 μm. **D**, Quantification of the relative migration distances of hCASMCs (n=3), obtained using ImageJ tool. One-way ANOVA with Bonferroni multiple comparison test was used to assess statistical significance indicated with *P* values. **E**, **F**, **G**, and **H**, Expression levels of dedifferentiation markers ACTA2 (actin alpha 2), MYH11 (myosin heavy chain 11) CD68, (cluster of differentiation 68), and LGALS3 (galectin 3) in hCASMCs (n=3) stimulated with water-soluble cholesterol-methyl-b-cyclodextrin (CMBCD) or 0.2% BSA for 72 h following transfection with GapCARMN, GapCTR or Mock. One-way ANOVA with Bonferroni multiple comparison test was used to assess statistical significance indicated with *P* values. UBC indicates ubiquitin C.

GapmeR, GapCARMN2 (Figure VIA through VIE in the Data Supplement). Collectively, these data suggest that the manipulation of the *CARMN* locus modulates the ability of hCASMCs to proliferate and migrate. In addition to this, the results obtained indicate that CARMN depletion affects the expression of some of the vSMC identity genes (*ACTA2* and *MYH11*) and increases the levels of some of the CMBCD-regulated genes (*CD68*, *ABCA1*, *ABCG1*) priming vSMC to a partial dedifferentiation process.

CARMN Depletion Regulates hCASMCs Proliferation in a miRNAs-Independent Manner

As the GapmeR strategy to downregulate CARMN also affects the expression of the miRNAs, we designed a rescue experiment to assess the contribution of both CARMN and the miRNAs to the described phenotypes. We have applied a cotransfection approach to overexpress the levels of miRNAs by treatment with miR-mimic (mimic-143 and mimic-145) in combination with GapmeR-mediated CARMN knockdown. We first assessed the efficiency of this strategy confirming a significant upregulation in the expression of both miRNAs by qRT-PCR (Figure 4A). Moreover, to assess their functional effect, we checked the expression of 2 miRNAs targets, *EGFR* (epidermal growth factor receptor) and *PDGFRa* (PDGF receptor alpha).[12,41] These were significantly downregulated following treatment with mimic-143 and mimic-145 (mimic-143/145) versus mimic control (mimicCTR; Figure VIF and VIG in the Data Supplement). In addition, we observed a significant upregulation of CARMN following treatment with miR-143/145 compared with mimic control. Although this increase might suggest a feedback loop in the modulation of CARMN expression induced by the hosted miRNAs (Figure 4B), this modulation did not restore CARMN expression to its basal levels. We then cotransfected hCASMCs in basal conditions with GapmeR targeting CARMN (GapCARMN) concomitantly with mimic control (mimicCTR) or a combination of mimic-143 and mimic-145. CARMN knockdown increased hCASMCs proliferation while the overexpression of miR-143 and miR-145 did not significantly change the observed increase in cell proliferation. Therefore, CARMN appears to have independent effect on the modulation of hCASMCs proliferation at basal conditions (Figure 4C). In contrast, miR-143/145 overexpression restored the levels of vSMC identity genes modulated by CARMN depletion, *ACTA2*, *MYH11* (Figure 4D, 4E, 4F, and 4G). In addition, the overexpression of miR-143/145 restored hCASMCs migration at basal levels thus rescuing the effects observed following CARMN depletion (Figure 4H and 4I). Taken together, these results suggest that CARMN can regulate hCASMCs proliferation independent of miR-143 and miR-145 but that migration and dedifferentiation may be driven through CARMN-mediated regulation of the miRNAs.

Expression of CARMN lncRNA and Associated miRNAs Are Downregulated in Mouse and Human Advanced Plaques

To determine the relevance of CARMN in human atherosclerosis, we assessed the expression of the lncRNA in atherosclerotic plaques isolated from symptomatic patients undergoing carotid endarterectomy. Previous analysis performed in stable and unstable regions of human plaques[8] were interrogated and revealed a significant decrease of CARMN levels in the unstable region versus the stable plaques (Figure 5A). Moreover, in the same RNA sequencing data, we interrogated the expression levels of previously identified CARMN-regulated genes. In agreement with the observations in CARMN knockdown samples, we found a significant upregulation of *MMP1*, significant downregulation of *ELN*, and a significant increase of proinflammatory genes (*IL1-beta* and *CCL2*; Figure 5B), in unstable versus stable plaques, confirming our findings from in vitro studies through to human atherosclerosis.

To validate these findings, we analyzed CARMN expression levels by qRT-PCR in carotid artery stenosis plaques isolated from different patients and confirmed the downregulation of the lncRNA in advanced versus early atheroma. Additionally, we showed the downregulation of miR-143 and miR-145 in the same samples (Figure 5C). To identify the cellular localization of CARMN within human plaques, in situ hybridization was performed in advanced stable plaques isolated from human carotid arteries of symptomatic patients. CARMN colocalized with α-*SMA* (α-smooth muscle actin), typical marker for vSMCs and with CD68, marker of macrophages and dedifferentiated vSMCs within the plaques (Figure 5D). Moreover, some CARMN RNAs colocalized with the CD45 marker[42] confirming the expression in immune cells. However, regions of the CD68/CARMN positive area appeared negative for *CD45* in parallel sections, suggesting the possibility of a nonimmune origin for these cells (Figure 5D).

As *CARMN* and miR-143/145 are evolutionary conserved, we were able to take advantage of mouse models to evaluate the expression and characterize the function of the CARMN locus. The mouse locus harbors 2 annotated isoforms of CARMN and their expression was analyzed using a common primer. To further examine the role of the CARMN in the pathophysiology of disease, we assessed the expression of the lncRNA and the miRNAs at different stages of murine atherosclerosis. For this purpose, we investigated the levels of the CARMN locus in 2 groups of low-density lipoprotein receptor knockout mice ($LDLR^{-/-}$): (1) mice fed with a 0.25% cholesterol diet for 14 weeks to develop advanced plaques and (2) mice fed on regular chow for 14 weeks to promote the formation of early fatty streak. We first confirmed the plaque stage

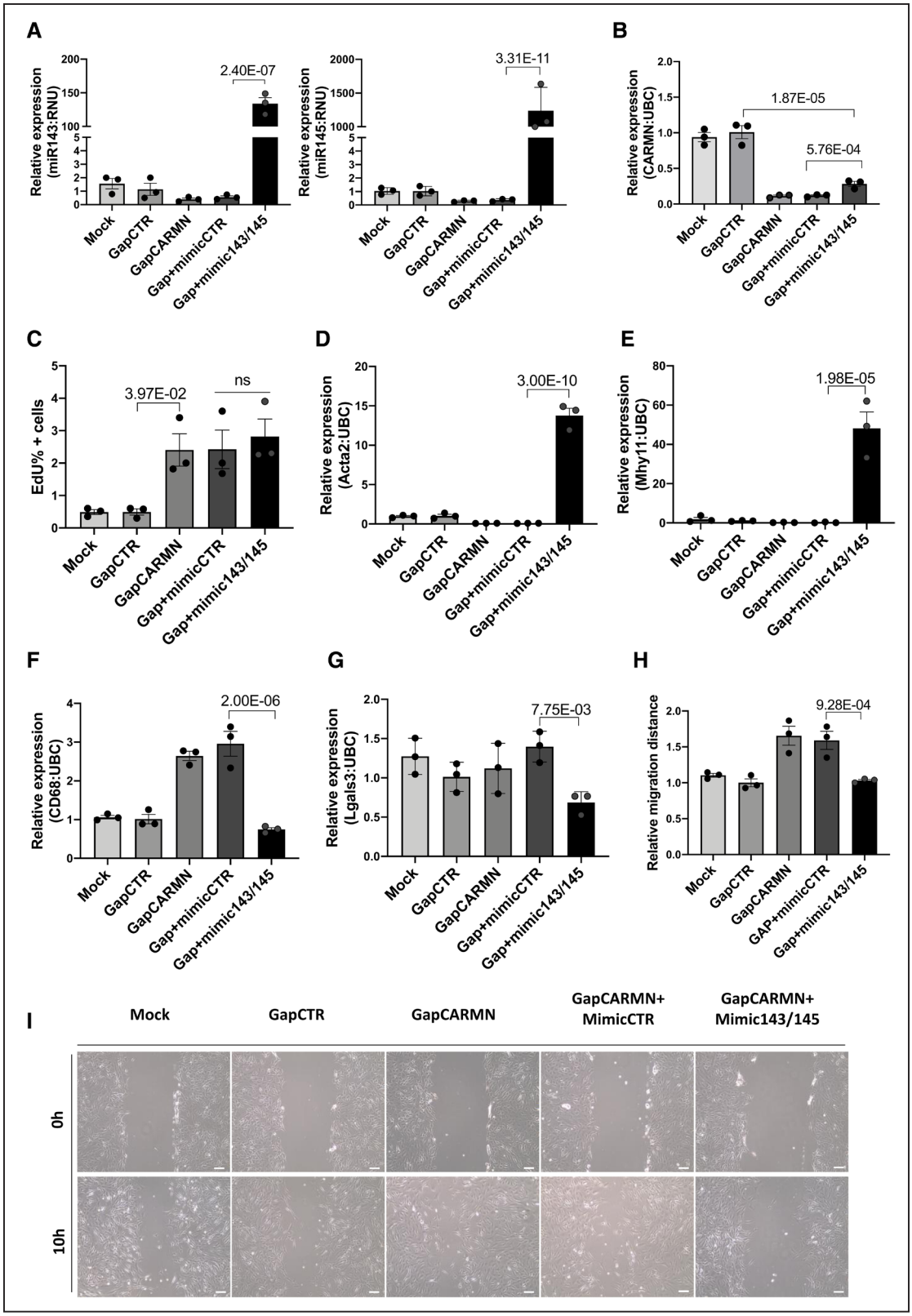

Figure 4. Cardiac mesoderm enhancer-associated noncoding RNA (CARMN) depletion regulated human coronary arterial smooth muscle cells (hCASMCs) phenotypes in microRNAs-dependent and independent mode.

A and **B**, Quantitative real-time polymerase chain reaction (qRT-PCR) expression data of microRNA-143 and -145 (miR-143 and miR-145) and CARMN relative to housekeeper gene RNU (small nucleolar RNA) and UBC (ubiquitin C), respectively) in locked nucleic acids antisense oligonucleotides (GapmeRs) targeting CARMN, (GapCARMN), control (GapCTR), a combination of GapCARMN and mimic control (Gap+mimicCTR) and a combination of GapCARMN and mimic overexpressing miR-143 and miR-145 (GapCARMN+mimic-143/145). Mock refers to untransfected control cells. One-way ANOVA with Bonferroni multiple (*Continued*)

through qualitative histological analysis classifying them as fatty streak, the first visible irregular lesion consisting of atherogenic lipoproteins and macrophages occurring at the lesion site,[43] or advanced atheroma, characterized by a large lipid-rich core, infiltrated macrophages, and thin collagen-poor fibrotic cap[44] (Figure 5E). Oil Red O staining was performed to confirm plaques stages (Figure VIIA in the Data Supplement).

We then isolated RNA from atherosclerotic lesions from each aortic root using laser capture microdissection, and assessed the expression levels of the lncRNA and miRNAs. The murine CARMN as well as miR-143 and miR-145 were found significantly downregulated in advanced lesions versus early plaques (Figure 5F), confirming the expression pattern observed in human advanced plaques.

CARMN-Axis Knockout Accelerates Atherosclerosis in Mice

Considering the decrease of CARMN in advanced human and murine plaques and in vitro vSMC functional data, we hypothesized that the loss of murine CARMN would modulate the development of atherosclerosis in vivo. Therefore, we exploited a CRISPR (clustered regularly interspaced short palindromic repeats)/Cas9 (CRISPR-associated protein 9)–mediated gene editing approach to constitutively knockout ($^{-/-}$) the *CARMN* locus. The first exon of the CARMN transcripts and a 4.8 kb portion of the gene promoter were deleted, leaving exons 2/3 and the miRNA stem-loops intact (Figure 6A). Aortas of mice on normal diet were used to confirm the deletion at the RNA level by RT-qPCR using primers directed at exon 1 versus wild-type controls CARMN wild-type (CARMN$^{+/+}$); Figure 6B. Using isoform-specific primers, downstream of the deletion site, we confirmed the knockdown of both transcripts (Figure VIIB and VIIC in the Data Supplement). We also observed in the same samples the downregulation of miR-143 and miR-145. Moreover, as part of the characterization of knockout mice, we examined the expression of the lncRNA Braveheart, downstream to CARMN transcript, which was previously found to be downregulated following loss of function of CARMN in mouse culture of cardiac progenitor cells (CPCs).[24] However, qRT-PCR data indicated that Braveheart expression was not significantly changed in aortic arches isolated from CARMN knockout (CARMN$^{-/-}$) versus CARMN$^{+/+}$ samples (Figure VIID in the Data Supplement). To determine the effect of CARMN deficiency in pathological context, we induced atherosclerosis in CARMN$^{-/-}$ mice and C57BL/6Ntac littermate controls using a validated mouse model of atherosclerosis[45,46] (Figure 6C). To achieve long-term hypercholesterolemia, 8-weeks old CARMN$^{+/+}$ and CARMN$^{-/-}$ mice were injected with 10^{12} vector genomes/mouse of the recombinant adeno-associated virus serotype 8 to induce overexpression of PCSK9 (proprotein convertase subtilisin/kexin type 9) in the liver. From one-week postinjection, all mice received high cholesterol diet for the following 18 weeks to promote hyperlipidemia and advanced atherosclerosis. Circulating cholesterol levels were measured at baseline (before virus administration), 6 and 10 weeks postinjection, and at euthanization. Consistent with previous studies validating the adeno-associated virus–PCSK9–induced model in wild-type animals,[46] we found increased cholesterol levels in CARMN$^{+/+}$ and CARMN$^{-/-}$ animals compared with baseline, demonstrating efficacy of the model (Figure VIIE in the Data Supplement). We found no differences in body weight and plasma cholesterol in CARMN$^{-/-}$ versus CARMN$^{+/+}$ animals (Figure VIIF and VIIG in the Data Supplement). Additionally, we did not observe significant differences in circulating immune cells and bone marrow progenitors in the 2 groups of animals, suggesting little or no effect on immune cell differentiation and proliferation (Figures VIII, IX, X in the Data Supplement). We next evaluated the severity of atherosclerosis by histological analysis in cross-sections in 2 of the main sites where atherosclerosis develops in mice, the brachiocephalic arteries and the aortic roots. To specifically evaluate the structure and the volume of the lesions in the brachiocephalic arteries, we used optical projection tomography.[47] Quantification of the resulting 3-dimensional images showed increased plaque volumes in CARMN$^{-/-}$ animals compared to wild-type controls (Figure 6D). Analysis of hematoxylin/eosin–stained section confirmed an increase in plaque area in the brachiocephalic arteries of CARMN$^{-/-}$ versus CARMN$^{+/+}$ mice (Figure 6E and 6F). Furthermore, we observed a significant increase in the cross-sectional area of the lesions developed in the aortic roots of CARMN$^{-/-}$ versus control mice (Figure 6G and 6H). We next sought to characterize the composition of the plaques in the brachiocephalic artery and aortic roots. In the pathological setting, abnormal proliferation of vSMCs[3,4] and resident

Figure 4 Continued. comparison test was used to assess statistical significance indicated with *P* values. **C**, Percentage of 5-ethynyl-2'-deoxyuridine (EdU) positive hCASMCs (n=3) evaluated by fluorescence-activated cell sorting (FACS) analysis and analyzed using FlowJo software. One-way ANOVA with Bonferroni multiple comparison test was used to assess statistical significance indicated with *P* values. **D**, **E**, **F**, and **G**, QRT-PCR expression data relative to ACTA2 (actin alpha 2), MYH11 (myosin heavy chain 11), CD68 (cluster of differentiation 68), and LGALS3 (galectin 3), respectively relative to housekeeper gene UBC in the above-mentioned transfection conditions. One-way ANOVA with Bonferroni multiple comparison test was used to assess statistical significance indicated with *P* values. **H** and **I**, Quantification of the relative migration distances of hCASMCs (n=3) obtained using ImageJ tool and representative images of hCASMCs at 0 and 10 h from the induction of the scratch. Images acquired at ×10 magnification, scale bar 100 μm. One-way ANOVA with Bonferroni multiple comparison test was used to assess statistical significance indicated with *P* values. ns indicates not significant.

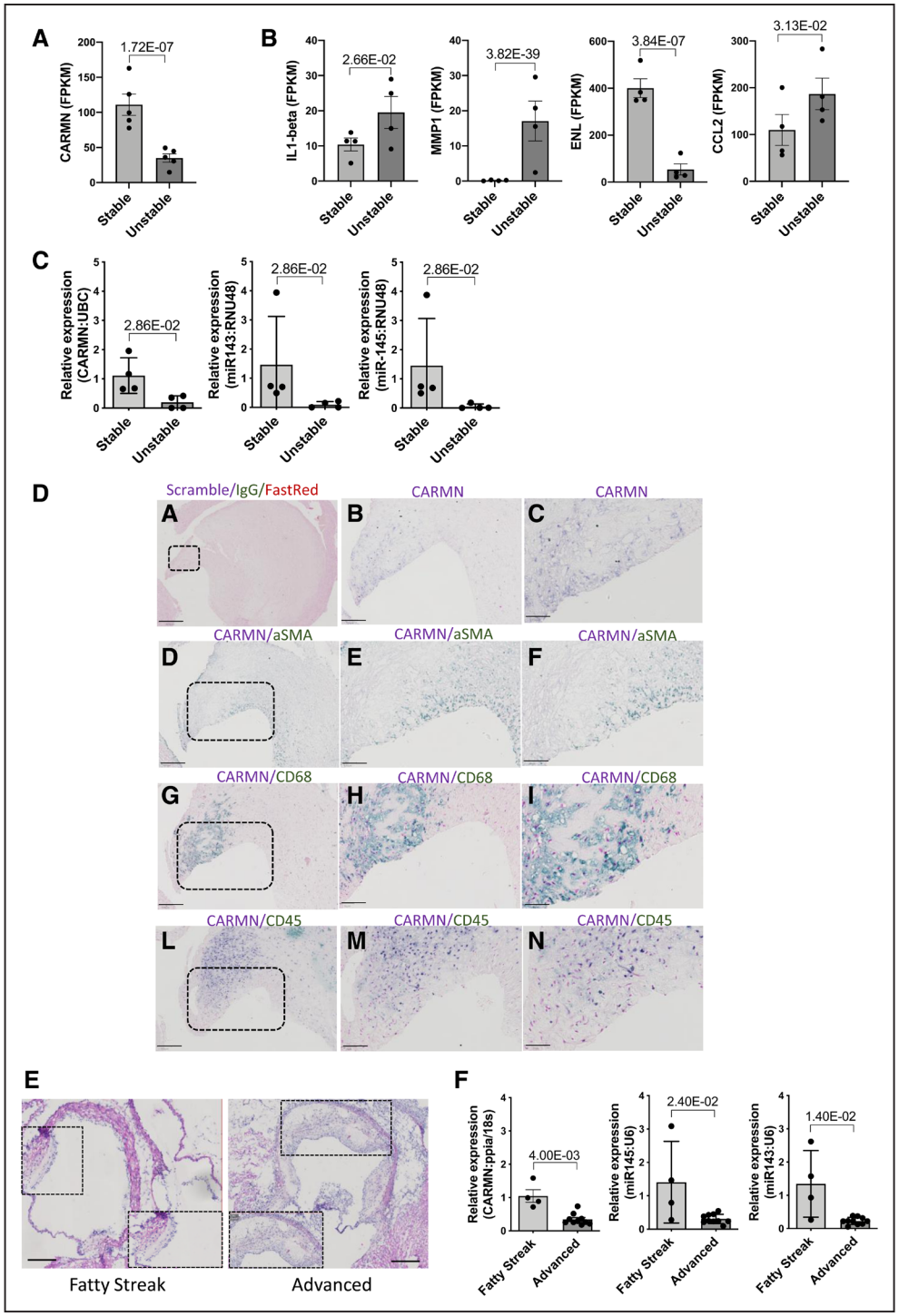

Figure 5. The cardiac mesoderm enhancer-associated noncoding RNA (CARMN) locus is downregulated in human and murine atherosclerosis.

A, Expression level of CARMN and (**B**) Expression level of MMP1 (matrix metalloproteinase 1), ELN (elastase), IL (interleukin) 1-beta, CCL (chemokine C-C motif ligand) 2 as FPKM, Fragments Per Kilobase of transcript per Million mapped reads in paired, stable (n=4) and unstable (n=4) human plaque segments retrieved after endarterectomy from 4 symptomatic patients. *P* value obtained based on the raw read counts using DESeq2. **C**, Expression of CARMN and microRNA-143 and -145 (miR-143 and miR-145) in human stable and unstable plaques isolated through endarterectomy (n=4) determined by quantitative real-time polymerase chain reaction. Mann-Whitney was used to assess statistical significance indicated with *P* values. **D**, Representative bright-field images of in situ detection of CARMN colocalizing with α-SMA (α smooth muscle actin), CD68, or CD45 signal in plaques obtained from carotid artery derived from symptomatic patients at carotid endarterectomy. Pictures were acquired consecutively at ×4, ×10, and ×40 magnification Scale bar 50 μm. **E**, Representative hematoxylin and eosin staining of aortic roots isolated from LDLR$^{-/-}$ mice. Pictures were acquired with ×4 and ×10 magnification. Scale bar 100 μm. **F**, Expression levels of CARMN and miR-143/145 in fatty streak (n=4) and advanced murine plaques (n=11) isolated by laser capture microdissection. Mann-Whitney was used to assess statistical significance indicated with *P* values. RNU indicates small nucleolar RNA; and UBC, ubiquitin C.

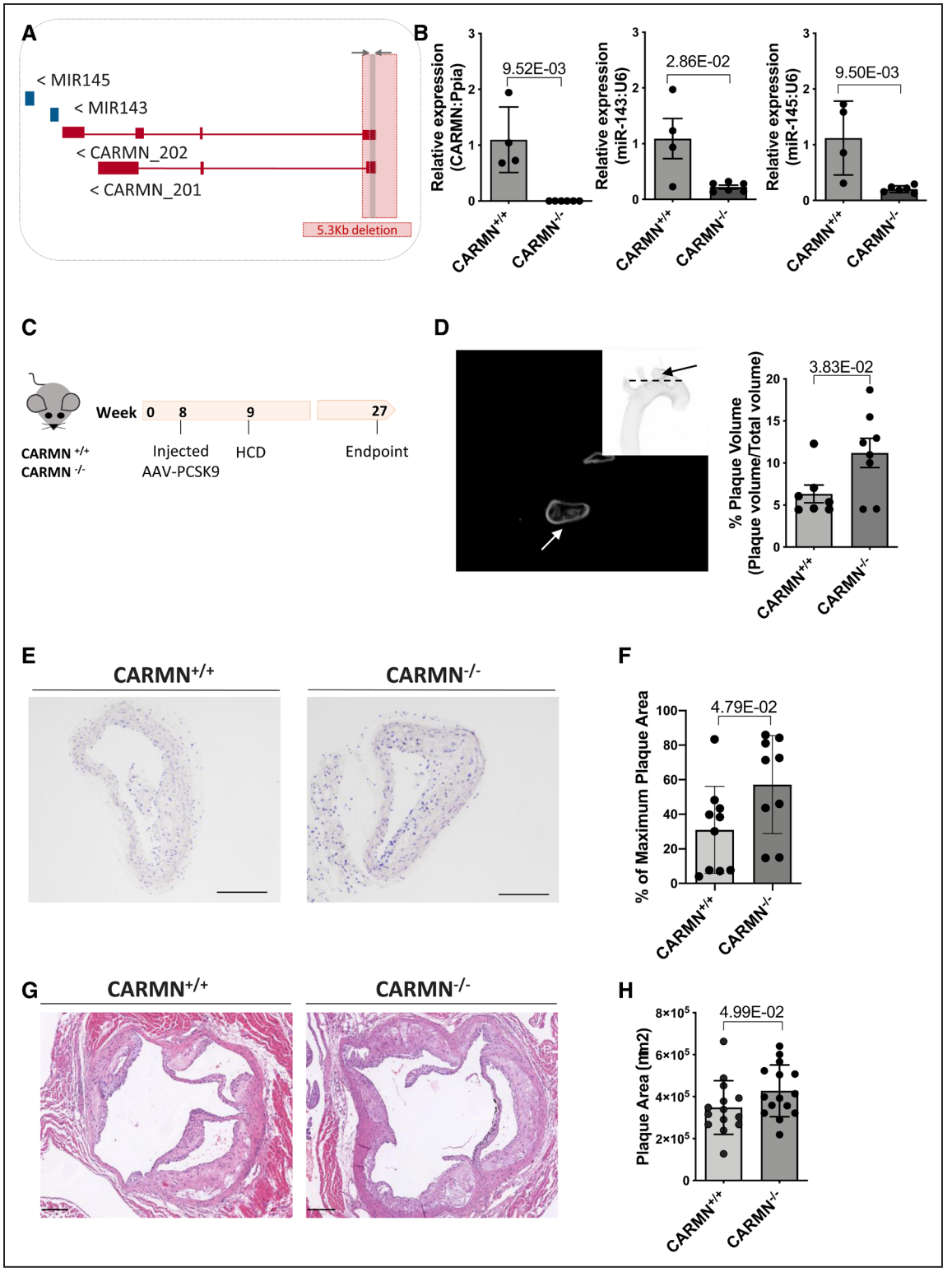

Figure 6. Genetic ablation of cardiac mesoderm enhancer-associated noncoding RNA (*CARMN*) affects the area, the volume, and the composition of plaques developed in the aortic arches of CARMN knockout (CARMN$^{-/-}$) vs CARMN wild-type (CARMN$^{+/+}$) animals.

A, Schematic representation of *CARMN* locus located on mouse chromosome 18 and the CRISPR (clustered regularly interspaced short palindromic repeats)/Cas9 (CRISPR-associated protein 9) deletion of the first exon and 4.8 kb of the promoter (total 5 kb). The arrows next to each transcript name indicate the direction of transcription. The gray arrows and box indicate where common primers to both isoforms were designed. **B**, Validation of knockout strategy by quantitative real-time polymerase chain reaction using common primer set performed on the aortic arches of CARMN$^{+/+}$ (n=4) and CARMN$^{-/-}$ (n=6) mice. Mann-Whitney was used to assess statistical significance indicated with *P* values. **C**, Schematic workflow used for the induction of mouse atherosclerosis using adeno-associated virus serotype 8 (AAV8)–mediated overexpression of PCSK9 (proprotein convertase subtilisin/kexin type 9) and high (*Continued*)

macrophages[48,49] represent key features of developing plaques. Cellular proliferation was analyzed by 5-ethynyl-2'-deoxyuridine incorporation. A significant increase in 5-ethynyl-2'-deoxyuridine incorporation was observed in the plaques of CARMN$^{-/-}$ animals compared to controls (Figure 7A and 7B) and thus increased proliferation rate of cells within the plaques. To further analyze the cellular composition of the plaques, cross-sections of the brachiocephalic arteries were stained for markers of vSMCs Acta2, Myh11, and a marker for activated macrophages and dedifferentiated vSMCs, Lgals3. Although the overall amount of smooth muscle actin-expressing vSMCs and cells positive for Myh11 was similar among the CARMN$^{+/+}$ and CARMN$^{-/-}$ groups (Figure 7C and 7D and Figure XC and XD in the Data Supplement), the content of Lgals3 in the plaque was found to be significantly increased in the lesions of CARMN$^{-/-}$ versus wild-type controls (Figure 7E and 7F). Moreover, the process of collagen deposition/degradation is a determinant factor in evaluating the structure and the stability of the plaques and can be used as measure of plaque vulnerability.[50,51] Therefore, we investigated the impact of CARMN$^{-/-}$ on the collagen turnover. Picrosirius red staining of the brachiocephalic arteries showed a significant decrease in collagen in CARMN$^{-/-}$ versus CARMN$^{+/+}$ animals, in line with decreased collagen gene expression observed in vitro. (Figure 7G and 7H). However, no significant change was observed in the plaque composition of the aortic roots of CARMN$^{-/-}$ versus wild-type controls (Figure VIIH through VIIK in the Data Supplement). The absence of significant differences between the CARMN$^{-/-}$ and CARMN$^{+/+}$ groups at the aortic root level could be explained by the vascular-site specific or temporal differences during plaque formation.[52] Overall, these data suggest that the depletion of *CARMN* induced the progression of atherosclerotic lesions to a more vulnerable plaque type.

DISCUSSION

Here, we comprehensively characterized for the first time the expression and function of the CARMN lncRNA loci in hCASMC phenotypes in vitro identified the functional consequence of the genetic loss of this lncRNA in the pathological setting of atherosclerosis in vivo. We show that GapmeR-mediated loss of the lncRNA primes vSMCs into a pro-pathological activated state, with concomitant reduction in the expression levels of both miR-143 and miR-145. Moreover, we functionally dissected the roles of CARMN and the miR-143/145 cluster, and highlighted that in addition to its role as microRNA host gene, our data suggest that the CARMN lncRNA has miRNA-independent effects on vSMCs function. Furthermore, we show loss of CARMN in advanced human and mouse atherosclerotic lesions compared to matched tissue with stable and less advanced disease regions. Finally, we show that CRISPR/Cas9–mediated genetic targeting of *CARMN* in mice leads to development of more advanced lesions in cholesterol-fed mice.

We used an RNA sequencing approach to understand the functional consequence of the modulation of CARMN lncRNA expression in vitro in hCASMCs. Our results revealed that the loss of CARMN lncRNA expression significantly affects the transcriptional vSMC landscape. In particular, following CARMN knockdown, hCASMCs gained a gene expression signature associated with a partially differentiated state towards a more plastic phenotype and showed a dysregulation of fundamental biological processes such as proliferation and migration. Transcriptomic analysis of CARMN at basal condition showed a substantial overlap with CMBCD-loaded signature, particularly in depleted cells and homeostasis of lipids. Accordingly, we postulated that depletion of CARMN predisposes hCASMCs to acquire early phenotypic/functional properties of foam cell–like cells, thus priming the proatherogenic phenotype likely contributing to the pathophysiology of cardiovascular disease. However, the dedifferentiation process following CARMN and miR-143/145 depletion affected only some of the vSMC identity markers indicating a partial effect towards dedifferentiating phenotype.

Recent studies have begun to unravel the complex network of interactions between those miRNAs that are embedded within so-called host genes,[26] whose biogenesis can be mutually exclusive[27] or they can be coexpressed and exert independent functions.[28] In our study, we observed the expression of miR-143 and miR-145 was also affected by CARMN depletion. This effect could simply be due to the pri-miRNA precursor overlapping CARMN locus. On the other hand, it is also possible the existence of a regulatory circuit in which CARMN represents an additional level of post-transcriptional

Figure 6 Continued. high cholesterol diet (HCD) in CARMN$^{+/+}$ and CARMN$^{-/-}$ animals. **D**, Representative tomographic reconstruction of pictures obtained by optical projection tomography (black picture) and nontomographic projection of the mouse aortic arch (white picture). The arrows indicate the brachiocephalic artery. Quantification of the plaque volumes in CARMN$^{+/+}$ (n=7) and CARMN$^{-/-}$ (n=8) animals performed using CTan software. Student *t* test was used to assess statistical significance indicated with *P* values. **E**, Representative hematoxylin and eosin staining of cross-sections from brachiocephalic artery of CARMN$^{+/+}$ and CARMN$^{-/-}$ animals. Pictures acquired at ×10 magnification. Scale bar 200 μm. **F**, Quantification of the plaque areas at the site of maximum lesion of brachiocephalic arteries in CARMN$^{+/+}$ (n=10) and CARMN$^{-/-}$ (n=9) mice, performed using Fiji software. Student *t* test was used to assess statistical significance indicated with *P* values. **G**, Hematoxylin and eosin staining of cross-sections from aortic roots of wild-type and CARMN$^{-/-}$ animals. Pictures acquired at ×5 magnification. Scale bar 200 μm. **H**, Quantification of plaque area of aortic roots of CARMN$^{+/+}$ (n=14) and CARMN$^{-/-}$ (n=15) animals, performed using QuPath software. Student *t* test was used to assess statistical significance indicated with *P* values. Ppia indicates cyclophilin A.

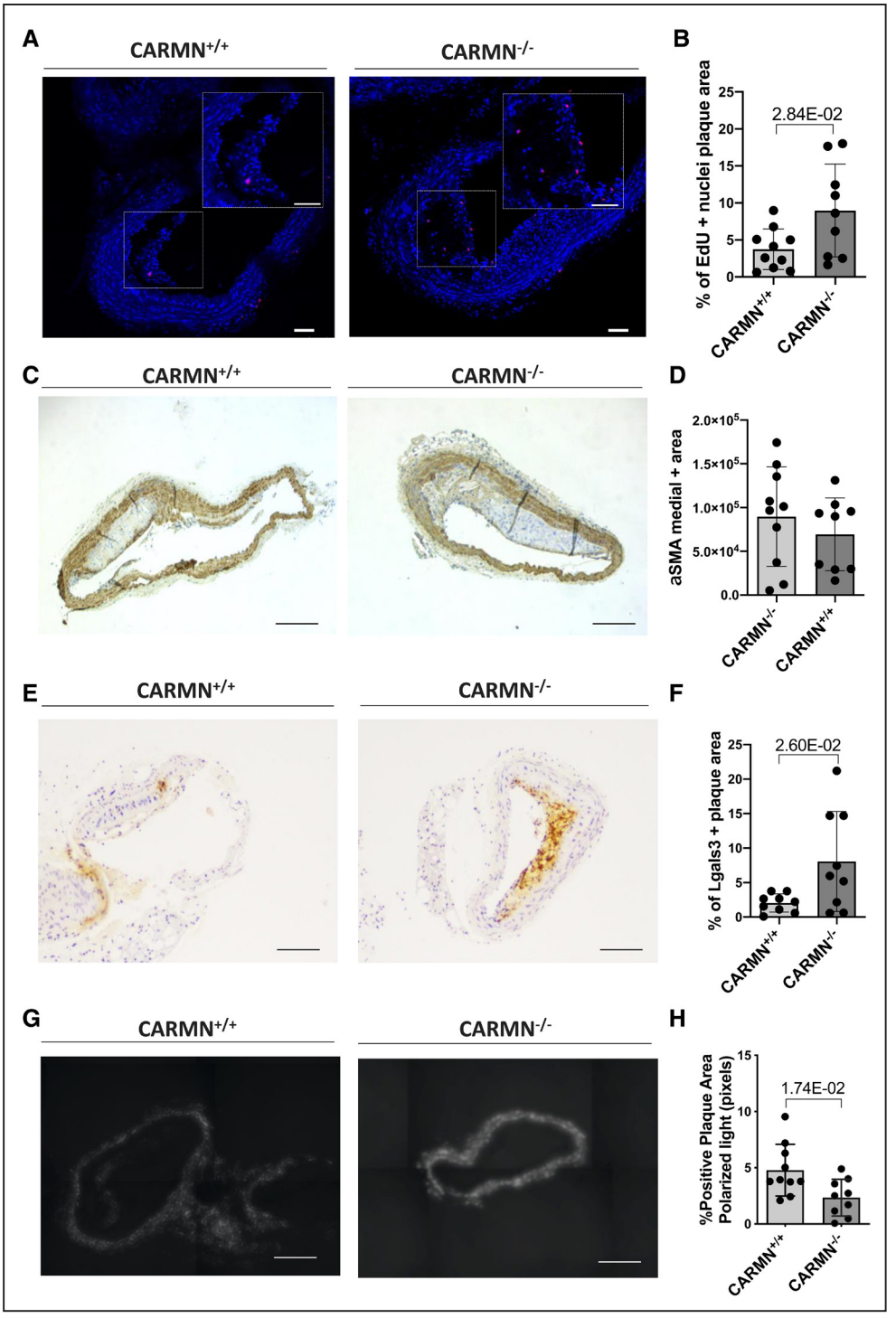

Figure 7. The genetic knockout of cardiac mesoderm enhancer-associated noncoding RNA (CARMN) increased the expression of Lgals3 (galectin 3) in plaques developed in the aortic arch of CARMN knockout (CARMN$^{-/-}$) animals vs wild-type controls. **A**, Representative 5-ethynyl-2'-deoxyuridine (EdU) staining of proliferating cells in plaques from CARMN wild-type (CARMN$^{+/+}$) and CARMN$^{-/-}$ animals. Pictures were acquired with ×10 magnification. Scale bar 80 μm. **B**, Quantification of proliferating cells in plaques of CARMN$^{+/+}$ (n=10) and CARMN$^{-/-}$ (n=9) animals. Values are expressed as % of positive nuclei over the total cells counted in the plaque. **C** and **E**, Representative immunostainings and (**D**) and (**F**) quantification of the positive area for αSMA (α smooth muscle actin) and Lgals3 staining respectively in the plaques of CARMN$^{+/+}$ (n=10) and CARMN$^{-/-}$ (n=9) animals. Pictures acquired at ×10 magnification. Scale bar 200 μm. **G**, Representative picrosirius red staining and (**H**) quantification of collagen content in the plaques of CARMN$^{+/+}$ (n=10) and CARMN$^{-/-}$ (n=9) animals. The pictures were acquired by polarized light microscopy at ×10 magnification. Scale bar 200 μm. Student *t* test was used to assess statistical significance indicated with *P* values.

regulation and its downregulation affects the expression level of the miRNAs. We acknowledge that the presence of multiple promoters identified for the miRNAs[16,20] enhances the challenge to uncover the existing lncRNA-miRNAs regulatory mechanisms. A recent study highlighted the possibility for lncRNA host genes to regulate hosted miRNAs via super-enhancer regulatory regions[53] and CARMN was previously shown to be associated with a super-enhancer region and to increase its activity.[24] However, the demonstration of the cisregulatory role of CARMN in vSMCs would require further studies, including chromatin marks and interaction analysis in this cell type. In addition, the literature on the regulation and function of these miRNAs in atherosclerosis is unclear.

We used a cotransfection strategy to increase the levels of miR-143/145 in CARMN-depleted vSMCs, allowing to dissect the contribution of CARMN from the miRNAs in vitro. Albeit the off-target limitation of the cotransfection strategy, our findings suggest that CARMN regulation of vSMC proliferation may possibly occur independently of the modulation of miR-143/145 expression. However, further dissociation of CARMN and miR-143 and miR-145 effect remains experimentally challenging due to the genetic complexity of the locus. Hence, further studies are required to understand the independent effects of CARMN and mir-143/145 using, for example, targeted CRISPR activation, inhibition, and editing approaches on the locus in primary vascular cells and mice. Our data expand the knowledge on the expression of the lncRNA at early and advanced stages of human and mouse atherosclerotic plaques. In a clinical setting, CARMN was significantly downregulated in advanced plaques versus stable lesions isolated by endarterectomy from symptomatic patients. Additionally, CARMN expression was found significantly reduced in murine advanced atheroma versus fatty streak. Therefore, we suggest that the downregulation of CARMN is a key event associated with the progression to more advanced lesions in cardiovascular disease.

To determine whether the functional role of the lncRNA is conserved in vivo, and to understand the functional consequence of the loss of CARMN during the pathophysiology of atherosclerosis in vivo, we genetically modulated the expression of the lncRNA in mice exploiting the CRISPR/Cas9 technology. Previous studies have genetically ablated a region of the pre-miRNAs stem-loop to generate miR-143/145-deficient mice.[14,15,17,19] We targeted the promoter region of the locus encompassing the first exon of CARMN transcripts. This resulted in the first genetic CARMN$^{-/-}$ model. In our in vivo atherosclerosis study using CARMN$^{-/-}$ mice, we found increased cellular proliferation in the atherosclerotic lesions of CARMN$^{-/-}$ versus CARMN$^{+/+}$ animals and a more advanced plaque phenotype in the CARMN$^{-/-}$ mice. This result can be explained by findings from previous studies where vSMCs within advanced plaque show high proliferative index.[54,55,56] The evaluation of plaque composition revealed a largely unchanged content of typical vSMC markers, *α-SMA* and *MYH11*. However, considering that expression of vSMC differentiation markers, such as *α-SMA* and *Myh11*, are lost by dedifferentiated vSMCs in advanced plaques,[7] the interpretation of these results is limited as vSMC may no longer be recognized as such. Recent advances in vSMC-fate mapping have allowed a more reliable identification of vSMC-derived cells which contribute to intimal and atherosclerotic lesions formation in injured arteries.[57,58] We acknowledge the lack of lineage-tracing mouse model represents a limitation to unambiguously characterize the plaque composition in our in vivo study. The evaluation of Lgals3 marker for macrophages and dedifferentiated vSMCs, revealed a significant increase in CARMN$^{-/-}$ versus CARMN$^{+/+}$ animals. Recently, studies have provided evidence that the rapid turnover and buildup of macrophages in advanced atherosclerotic plaques is mostly due to their local proliferation.[48,59] Importantly, the large pool of foamy and proinflammatory cells expressing Lgals3, was defined among the main features of lesion progression toward the advanced state.[38] Accordingly, our results show that CARMN$^{-/-}$ increases the content of Lgals3, thus inducing the progression of the plaques toward an inflammatory and advanced stage. Collectively, these results reveal the functional role of CARMN-axis to the phenotype observed in vivo and to clearly define the contribution of CARMN and microRNAs separately is an area for future research.

The decrease in collagen content within the lesions has been associated with progression to a more advanced plaque phenotype.[60] In this context, previous studies have reported that lower content of collagen may be due to a reduced synthesis by vSMCs and to an enhanced degradation by metalloproteases and collagenases.[50] In our study, the analysis of total collagen content within the plaques showed a significant decrease in CARMN$^{-/-}$ versus CARMN$^{+/+}$ mice, confirming that CARMN$^{-/-}$ induced a more advanced plaque phenotype. These results are consistent with the transcriptomic analysis of hCASMCs following knockdown of CARMN, where we observed a decrease in collagen and elastase gene expression and the upregulation of genes associated with collagen breakdown (MMPs [metalloproteases]).

Collectively, our study demonstrates that loss of CARMN-axis is an early event in atherosclerosis, both in mice and humans. We have shown that downregulation of CARMN is detrimental for the maintenance of hCASMCs differentiated state and induces itself a phenotypic transition toward proproliferative phenotype, independently from the modulation of miR-143/145 cluster. In this research, we have characterized the effect of the dysregulation of miR-143/145 on the expression of vSMC identity genes and their ability to migrate. Finally, we have characterized the phenotypic consequence of *CARMN* depletion during the development of atherosclerosis in vivo and demonstrated that the knockout of

CARMN locus altered the composition of the plaques to a more advanced plaque type.

ARTICLE INFORMATION

Received December 15, 2020; revision received February 17, 2021; accepted February 23, 2021.

Affiliations

Queens Medical Research Institute, BHF Centre for Cardiovascular Sciences (F.V., J.R., M.K.L., A.D.M., M.B., E.M., J.P.S., D.E.N., P.W.F.H., L.D., J.C.S., A.H.B.), Institute for Regeneration and Repair, Centre for Regenerative Medicine (A.D.P., D.O.), and Insitute of Genetics and Molecular Medicine (T.C.W.), University of Edinburgh, Scotland. Pathology, Maastricht Medical Center, the Netherlands (K.V.K., J.d., J.C.S., A.H.B.). Medical Biochemistry, Experimental Vascular Biology, Amsterdam UMC, University of Amsterdam, the Netherlands (M. Gijbels). Pathology CARIM, Cardiovascular Research Institute Maastricht, GROW-School for Oncology and Developmental Biology, Maastricht University, the Netherlands (M. Gijbels). Centre for Stem Cell Systems, Department of Anatomy and Neuroscience, The University of Melbourne, Australia (M.B.C.). Medicine, Vanderbilt University Medical Center, Nashville, Tennessee (A.C.D). miRagen Therapeutics, Inc, Boulder, Colorado (R.M.). King's College London, England (M. Giacca).

Acknowledgments

We thank Gregor Aitchison, Kathryn Newton, Michael Millar, Erwin Wijnands, and George Kuriakose for their technical assistance during the study. Flow cytometry data were generated with support from the QMRI Flow Cytometry and cell sorting facility, University of Edinburgh. adeno-associated virus serotype 8 (AAV8)-PCSK9 (proprotein convertase subtilisin/kexin type 9) was kindly provided by the AVU (AAV Vector Unit), I.C.G.E.B (Trieste, TS). Laser Capture Microdissection was performed in collaboration with Professor Ira Tabas at Columbia University Medical Centre (NY) and with the technical assistance of the Confocal and Specialized Microscopy Shared Resource, Columbia University Medical Centre (NY). The authors also thank Professor Martyn Taylor, Stefan Rooke, and Amanda Warr for the assistance provided during the Oxford Nanopore sequencing and data analysis.

Sources of Funding

This work is supported by the British Heart Foundation (BHF) Research Excellent Award (RE/18/5/34216), BHF Chair (CH/11/2/28733) and fellowship to F. Vacante (FS/18/10/33413), and a BHF programme Grant to A.H. Baker (BHF CVR grant [RM/17/3/33381]) and the European Research Council Advanced Grant VASMIR (RE7644) to A.H. Baker and Dutch heart foundation fellowship 2016T060 and a Leducq transatlantic network grant to J.C. Sluimer and BHF project grant to A.H. Baker and L. Denby. This project has also received funding from the European Union's Horizon 2020 Programme for Research and Innovation (825670). T.C. Williams is the recipient of a Wellcome Trust award (204802/Z/16/Z). Australian National Health and Medical Research Council Early Career Fellowship (APP1072662 to M.B. Clark).

Disclosures

M.B. Clark has received support from Oxford Nanopore Technologies (ONT) to present at scientific conferences. However, ONT played no role in study design, execution, analysis, or publication. The other authors report no conflicts.

Supplemental Materials

Expanded Methods
Data Supplement Figures I–X
Dataset I–VI

REFERENCES

1. Stefanadis C, Antoniou CK, Tsiachris D, Pietri P. Coronary atherosclerotic vulnerable plaque: current perspectives. *J Am Heart Assoc*. 2017;6:e005543. doi: 10.1161/JAHA.117.005543
2. Owens GK, Kumar MS, Wamhoff BR. Molecular regulation of vascular smooth muscle cell differentiation in development and disease. *Physiol Rev*. 2004;84:767–801. doi: 10.1152/physrev.00041.2003
3. Gomez D, Owens GK. Smooth muscle cell phenotypic switching in atherosclerosis. *Cardiovasc Res*. 2012;95:156–164. doi: 10.1093/cvr/cvs115
4. Bennett MR, Sinha S, Owens GK. Vascular smooth muscle cells in atherosclerosis. *Circ Res*. 2016;118:692–702. doi: 10.1161/CIRCRESAHA.115.306361
5. Wang Y, Dubland JA, Allahverdian S, Asonye E, Sahin B, Jaw JE, Sin DD, Seidman MA, Leeper NJ, Francis GA. Smooth muscle cells contribute the majority of foam cells in ApoE (apolipoprotein E)-deficient mouse atherosclerosis. *Arterioscler Thromb Vasc Biol*. 2019;39:876–887. doi: 10.1161/ATVBAHA.119.312434
6. Newby AC, Zaltsman AB. Fibrous cap formation or destruction - the critical importance of vascular smooth muscle cell proliferation, migration and matrix formation. *Cardiovasc Res*. 1999;41:345–360.
7. Allahverdian S, Chaabane C, Boukais K, Francis GA, Bochaton-Piallat ML. Smooth muscle cell fate and plasticity in atherosclerosis. *Cardiovasc Res*. 2018;114:540–550. doi: 10.1093/cvr/cvy022
8. Mahmoud AD, Ballantyne MD, Miscianinov V, Pinel K, Hung J, Scanlon JP, Iyinikkel J, Kaczynski J, Tavares AS, Bradshaw AC, et al. The human-specific and smooth muscle cell-enriched LncRNA SMILR promotes proliferation by regulating mitotic CENPF mRNA and drives cell-cycle progression which can be targeted to limit vascular remodeling. *Circ Res*. 2019;125:535–551. doi: 10.1161/CIRCRESAHA.119.314876
9. Cremer S, Michalik KM, Fischer A, Pfisterer L, Jaé N, Winter C, Boon RA, Muhly-Reinholz M, John D, Uchida S, et al. Hematopoietic deficiency of the long noncoding RNA MALAT1 promotes atherosclerosis and plaque inflammation. *Circulation*. 2019;139:1320–1334. doi: 10.1161/CIRCULATIONAHA.117.029015
10. Hung J, Scanlon JP, Mahmoud AD, Rodor J, Ballantyne M, Fontaine MAC, Temmerman L, Kaczynski J, Connor KL, Bhushan R, et al. Novel plaque enriched long noncoding RNA in atherosclerotic macrophage regulation (PELATON). *Arterioscler Thromb Vasc Biol*. 2020;40:697–713. doi: 10.1161/ATVBAHA.119.313430
11. Vengrenyuk Y, Nishi H, Long X, Ouimet M, Savji N, Martinez FO, Cassella CP, Moore KJ, Ramsey SA, Miano JM, et al. Cholesterol loading reprograms the microRNA-143/145-myocardin axis to convert aortic smooth muscle cells to a dysfunctional macrophage-like phenotype. *Arterioscler Thromb Vasc Biol*. 2015;35:535–546. doi: 10.1161/ATVBAHA.114.304029
12. Quintavalle M, Elia L, Condorelli G, Courtneidge SA. MicroRNA control of podosome formation in vascular smooth muscle cells in vivo and in vitro. *J Cell Biol*. 2010;189:13–22. doi: 10.1083/jcb.200912096
13. Vacante F, Denby L, Sluimer JC, Baker AH. The function of miR-143, miR-145 and the MiR-143 host gene in cardiovascular development and disease. *Vascul Pharmacol*. 2019;112:24–30. doi: 10.1016/j.vph.2018.11.006
14. Boettger T, Beetz N, Kostin S, Schneider J, Krüger M, Hein L, Braun T. Acquisition of the contractile phenotype by murine arterial smooth muscle cells depends on the miR143/145 gene cluster. *J Clin Invest*. 2009;119:2634–2647. doi: 10.1172/JCI38864
15. Elia L, Quintavalle M, Zhang J, Contu R, Cossu L, Latronico MV, Peterson KL, Indolfi C, Catalucci D, Chen J, et al. The knockout of miR-143 and -145 alters smooth muscle cell maintenance and vascular homeostasis in mice: correlates with human disease. *Cell Death Differ*. 2009;16:1590–1598. doi: 10.1038/cdd.2009.153
16. Cordes KR, Sheehy NT, White MP, Berry EC, Morton SU, Muth AN, Lee TH, Miano JM, Ivey KN, Srivastava D. miR-145 and miR-143 regulate smooth muscle cell fate and plasticity. *Nature*. 2009;460:705–710. doi: 10.1038/nature08195
17. Xin M, Small EM, Sutherland LB, Qi X, McAnally J, Plato CF, Richardson JA, Bassel-Duby R, Olson EN. MicroRNAs miR-143 and miR-145 modulate cytoskeletal dynamics and responsiveness of smooth muscle cells to injury. *Genes Dev*. 2009;23:2166–2178. doi: 10.1101/gad.1842409
18. Lovren F, Pan Y, Quan A, Singh KK, Shukla PC, Gupta N, Steer BM, Ingram AJ, Gupta M, Al-Omran M, et al. MicroRNA-145 targeted therapy reduces atherosclerosis. *Circulation*. 2012;126:S81–S90. doi: 10.1161/CIRCULATIONAHA.111.084186
19. Cipollone F, Felicioni L, Sarzani R, Ucchino S, Spigonardo F, Mandolini C, Malatesta S, Bucci M, Mammarella C, Santovito D, et al. A unique microRNA signature associated with plaque instability in humans. *Stroke*. 2011;42:2556–2563. doi: 10.1161/STROKEAHA.110.597575
20. Deng L, Blanco FJ, Stevens H, Lu R, Caudrillier A, McBride M, McClure JD, Grant J, Thomas M, Frid M, et al. MicroRNA-143 activation regulates smooth muscle and endothelial cell crosstalk in pulmonary arterial hypertension. *Circ Res*. 2015;117:870–883. doi: 10.1161/CIRCRESAHA.115.306806
21. Caruso P, Dempsie Y, Stevens HC, McDonald RA, Long L, Lu R, White K, Mair KM, McClure JD, Southwood M, et al. A role for miR-145 in pulmonary arterial hypertension: evidence from mouse models and patient samples. *Circ Res*. 2012;111:290–300. doi: 10.1161/CIRCRESAHA.112.267591
22. Rangrez AY, Massy ZA, Metzinger-Le Meuth V, Metzinger L. miR-143 and miR-145: molecular keys to switch the phenotype of vascular smooth muscle cells. *Circ Cardiovasc Genet*. 2011;4:197–205. doi: 10.1161/CIRCGENETICS.110.958702

23. Lagarde J, Uszczynska-Ratajczak B, Carbonell S, Pérez-Lluch S, Abad A, Davis C, Gingeras TR, Frankish A, Harrow J, Guigo R, et al. High-throughput annotation of full-length long noncoding RNAs with capture long-read sequencing. *Nat Genet*. 2017;49:1731–1740. doi: 10.1038/ng.3988
24. Ounzain S, Micheletti R, Arnan C, Plaisance I, Cecchi D, Schroen B, Reverter F, Alexanian M, Gonzales C, Ng SY, et al. CARMEN, a human super enhancer-associated long noncoding RNA controlling cardiac specification, differentiation and homeostasis. *J Mol Cell Cardiol*. 2015;89:98–112. doi: 10.1016/j.yjmcc.2015.09.016
25. Plaisance I, Perruchoud S, Fernandez-Tenorio M, Gonzales C, Ounzain S, Ruchat P, Nemir M, Niggli E, Pedrazzini T. Cardiomyocyte lineage specification in adult human cardiac precursor cells via modulation of enhancer-associated long noncoding RNA expression. *JACC Basic Transl Sci*. 2016;1:472–493. doi: 10.1016/j.jacbts.2016.06.008
26. Profumo V, Forte B, Percio S, Rotundo F, Doldi V, Ferrari E, Fenderico N, Dugo M, Romagnoli D, Benelli M, et al. LEADeR role of miR-205 host gene as long noncoding RNA in prostate basal cell differentiation. *Nat Commun*. 2019;10:307. doi: 10.1038/s41467-018-08153-2
27. Legnini I, Morlando M, Mangiavacchi A, Fatica A, Bozzoni I. A feedforward regulatory loop between HuR and the long noncoding RNA linc-MD1 controls early phases of myogenesis. *Mol Cell*. 2014;53:506–514. doi: 10.1016/j.molcel.2013.12.012
28. Sun Q, Tripathi V, Yoon JH, Singh DK, Hao Q, Min KW, Davila S, Zealy RW, Li XL, Polycarpou-Schwarz M, et al. MIR100 host gene-encoded lncRNAs regulate cell cycle by modulating the interaction between HuR and its target mRNAs. *Nucleic Acids Res*. 2018;46:10405–10416. doi: 10.1093/nar/gky696
29. Ulitsky I, Bartel DP. lincRNAs: genomics, evolution, and mechanisms. *Cell*. 2013;154:26–46. doi: 10.1016/j.cell.2013.06.020
30. Ponting CP, Oliver PL, Reik W. Evolution and functions of long noncoding RNAs. *Cell*. 2009;136:629–641. doi: 10.1016/j.cell.2009.02.006
31. Deaton RA, Gan Q, Owens GK. Spl-dependent activation of KLF4 is required for PDGF-BB-induced phenotypic modulation of smooth muscle. *Am J Physiol Hear Circ Physiol*. 2009;296:H1027–H1037. doi: 10.1152/ajpheart.01230.2008
32. Chellan B, Reardon CA, Getz GS, Hofmann Bowman MA. Enzymatically modified low-density lipoprotein promotes foam cell formation in smooth muscle cells via macropinocytosis and enhances receptor-mediated uptake of oxidized low-density lipoprotein. *Arterioscler Thromb Vasc Biol*. 2016;36:1101–1113. doi: 10.1161/ATVBAHA.116.307306
33. Miano JM. Myocardin in biology and disease. *J Biomed Res*. 2015;29:3–19. doi: 10.7555/JBR.29.20140151
34. Ait-Oufella H, Taleb S, Mallat Z, Tedgui A. Recent advances on the role of cytokines in atherosclerosis. *Arterioscler Thromb Vasc Biol*. 2011;31:969–979. doi: 10.1161/ATVBAHA.110.207415
35. van der Vorst EP, Döring Y, Weber C. Chemokines and their receptors in atherosclerosis. *J Mol Med (Berl)*. 2015;93:963–971. doi: 10.1007/s00109-015-1317-8
36. Adiguzel E, Ahmad PJ, Franco C, Bendeck MP. Collagens in the progression and complications of atherosclerosis. *Vasc Med*. 2009;14:73–89. doi: 10.1177/1358863X08094801
37. Newby AC. Metalloproteinases and vulnerable atherosclerotic plaques. *Trends Cardiovasc Med*. 2007;17:253–258. doi: 10.1016/j.tcm.2007.09.001
38. Shankman LS, Gomez D, Cherepanova OA, Salmon M, Alencar GF, Haskins RM, Swiatlowska P, Newman AA, Greene ES, Straub AC, et al. KLF4-dependent phenotypic modulation of smooth muscle cells has a key role in atherosclerotic plaque pathogenesis. *Nat Med*. 2015;21:628–637. doi: 10.1038/nm.3866
39. Duband JL, Gimona M, Scatena M, Sartore S, Small JV. Calponin and SM 22 as differentiation markers of smooth muscle: spatiotemporal distribution during avian embryonic development. *Differentiation*. 1993;55:1–11. doi: 10.1111/j.1432-0436.1993.tb00027.x
40. Zhang H, Jiang M, Liu Q, Han Z, Zhao Y, Ji S. miR-145-5p inhibits the proliferation and migration of bladder cancer cells by targeting TAGLN2. *Oncol Lett*. 2018;16:6355–6360. doi: 10.3892/ol.2018.9436
41. Zhu H, Dougherty U, Robinson V, Mustafi R, Pekow J, Kupfer S, Li YC, Hart J, Goss K, Fichera A, et al. EGFR signals downregulate tumor suppressors miR-143 and miR-145 in Western diet-promoted murine colon cancer: role of G1 regulators. *Mol Cancer Res*. 2011;9:960–975. doi: 10.1158/1541-7786.MCR-10-0531
42. Koltsova EK, Hedrick CC, Ley K. Myeloid cells in atherosclerosis: a delicate balance of anti-inflammatory and proinflammatory mechanisms. *Curr Opin Lipidol*. 2013;24:371–380. doi: 10.1097/MOL.0b013e328363d298
43. Stary HC, Chandler AB, Glagov S, Guyton JR, Insull W Jr, Rosenfeld ME, Schaffer SA, Schwartz CJ, Wagner WD, Wissler RW. A definition of initial, fatty streak, and intermediate lesions of atherosclerosis. A report from the Committee on Vascular Lesions of the Council on Arteriosclerosis, American Heart Association. *Arterioscler Thromb*. 1994;14:840–856. doi: 10.1161/01.atv.14.5.840
44. Falk E. Pathogenesis of atherosclerosis. *J Am Coll Cardiol*. 2006;47:C7–12. doi: 10.1016/j.jacc.2005.09.068
45. Maxwell KN, Breslow JL. Adenoviral-mediated expression of Pcsk9 in mice results in a low-density lipoprotein receptor knockout phenotype. *Proc Natl Acad Sci U S A*. 2004;101:7100–7105. doi: 10.1073/pnas.0402133101
46. Bjørklund MM, Hollensen AK, Hagensen MK, Dagnaes-Hansen F, Christoffersen C, Mikkelsen JG, Bentzon JF. Induction of atherosclerosis in mice and hamsters without germline genetic engineering. *Circ Res*. 2014;114:1684–1689. doi: 10.1161/CIRCRESAHA.114.302937
47. Kirkby NS, Low L, Seckl JR, Walker BR, Webb DJ, Hadoke PW. Quantitative 3-dimensional imaging of murine neointimal and atherosclerotic lesions by optical projection tomography. *PLoS One*. 2011;6:e16906. doi: 10.1371/journal.pone.0016906
48. Robbins CS, Hilgendorf I, Weber GF, Theurl I, Iwamoto Y, Figueiredo JL, Gorbatov R, Sukhova GK, Gerhardt LM, Smyth D, et al. Local proliferation dominates lesional macrophage accumulation in atherosclerosis. *Nat Med*. 2013;19:1166–1172. doi: 10.1038/nm.3258
49. Jenkins SJ, Ruckerl D, Thomas GD, Hewitson JP, Duncan S, Brombacher F, Maizels RM, Hume DA, Allen JE. IL-4 directly signals tissue-resident macrophages to proliferate beyond homeostatic levels controlled by CSF-1. *J Exp Med*. 2013;210:2477–2491. doi: 10.1084/jem.20121999
50. Rekhter MD. Collagen synthesis in atherosclerosis: too much and not enough. *Cardiovasc Res*. 1999;41:376–384. doi: 10.1016/s0008-6363(98)00321-6
51. Rekhter MD. How to evaluate plaque vulnerability in animal models of atherosclerosis? *Cardiovasc Res*. 2002;54:36–41. doi: 10.1016/s0008-6363(01)00537-5
52. VanderLaan PA, Reardon CA, Getz GS. Site specificity of atherosclerosis: site-selective responses to atherosclerotic modulators. *Arterioscler Thromb Vasc Biol*. 2004;24:12–22. doi: 10.1161/01.ATV.0000105054.43931.f0
53. Suzuki HI, Young RA, Sharp PA. Super-enhancer-mediated RNA processing revealed by integrative microRNA network analysis. *Cell*. 2017;168:1000–1014.e15. doi: 10.1016/j.cell.2017.02.015
54. Doran AC, Meller N, McNamara CA. Role of smooth muscle cells in the initiation and early progression of atherosclerosis. *Arterioscler Thromb Vasc Biol*. 2008;28:812–819. doi: 10.1161/ATVBAHA.107.159327
55. Chappell J, Harman JL, Narasimhan VM, Yu H, Foote K, Simons BD, Bennett MR, Jørgensen HF. Extensive proliferation of a subset of differentiated, yet plastic, medial vascular smooth muscle cells contributes to neointimal formation in mouse injury and atherosclerosis models. *Circ Res*. 2016;119:1313–1323. doi: 10.1161/CIRCRESAHA.116.309799
56. Dobnikar L, Taylor AL, Chappell J, Oldach P, Harman JL, Oerton E, Dzierzak E, Bennett MR, Spivakov M, Jørgensen HF. Publisher correction: disease-relevant transcriptional signatures identified in individual smooth muscle cells from healthy mouse vessels. *Nat Commun*. 2018;9:5401. doi: 10.1038/s41467-018-07887-3
57. Majesky MW, Horita H, Ostriker A, Lu S, Regan JN, Bagchi A, Dong XR, Poczobutt J, Nemenoff RA, Weiser-Evans MC. Differentiated smooth muscle cells generate a subpopulation of resident vascular progenitor cells in the adventitia regulated by Klf4. *Circ Res*. 2017;120:296–311. doi: 10.1161/CIRCRESAHA.116.309322
58. Feil S, Fehrenbacher B, Lukowski R, Essmann F, Schulze-Osthoff K, Schaller M, Feil R. Transdifferentiation of vascular smooth muscle cells to macrophage-like cells during atherogenesis. *Circ Res*. 2014;115:662–667. doi: 10.1161/CIRCRESAHA.115.304634
59. Lutgens E, de Muinck ED, Kitslaar PJ, Tordoir JH, Wellens HJ, Daemen MJ. Biphasic pattern of cell turnover characterizes the progression from fatty streaks to ruptured human atherosclerotic plaques. *Cardiovasc Res*. 1999;41:473–479. doi: 10.1016/s0008-6363(98)00311-3
60. Barnes MJ, Farndale RW. Collagens and atherosclerosis. *Exp Gerontol*. 1999;34:513–525. doi: 10.1016/s0531-5565(99)00038-8